Available online at www.sciencedirect.com

SciVerse ScienceDirect

Ceramics International 38 (2012) 2927–2934

CERAMICS INTERNATIONAL

www.elsevier.com/locate/ceramint

Microwave dielectric properties and microstructures of $Nd(Mg_{0.5}Sn_{0.5-x}Ti_x)O_3$ ceramics

Yih-Chien Chen *, Ren-Jie Tsai, Chung-Yen Wu

Department of Electrical Engineering, Lunghwa University of Science and Technology, Gueishan Shiang, Taoyuan County, Taiwan

Received 23 June 2011; received in revised form 30 October 2011; accepted 25 November 2011
Available online 6 December 2011

Abstract

This study elucidates the microwave dielectric properties and microstructures of $Nd(Mg_{0.5}Sn_{0.5-x}Ti_x)O_3$ ceramics with a view to their potential for microwave devices. The $Nd(Mg_{0.5}Sn_{0.5-x}Ti_x)O_3$ ceramics were prepared by the conventional solid-state method with various sintering temperatures. The X-ray diffraction patterns of the $Nd(Mg_{0.5}Sn_{0.4}Ti_{0.1})O_3$ ceramics revealed no significant variation of phase with sintering temperatures. A dielectric constant (ε_r) of 21.1, a quality factor ($Q \times f$) of 50,000 GHz, and a temperature coefficient of resonant frequency (τ_f) of -60 ppm/°C were obtained for $Nd(Mg_{0.5}Sn_{0.4}Ti_{0.1})O_3$ ceramics that were sintered at 1550 °C for 4 h.

Keywords: A. Sintering; C. Dielectric properties; Ceramic; X-ray diffraction

1. Introduction

The advantages provided by using complex perovskite ceramics $A(B'_{0.5}B''_{0.5})O_3$ ($A = Me^{2+}$, Me^{3+}; $B' = Me^{2+}$, Me^{3+}; $B'' = Me^{4+}$, Me^{5+}, Me^{6+}) are reportedly associated with their excellent microwave dielectric properties [1–7]. Many investigations of $Nd(Mg_{0.5}Sn_{0.5})O_3$ ceramics and related ceramic systems have investigated their potential application in resonators, filters and antennas in modern communication systems, such as radar and wireless local area network (WLAN), which are operated at microwave frequencies. A dielectric constant of 19.3, a $Q \times f$ of 43,300 GHz, and a temperature coefficient of resonant frequency of -57 ppm/°C were obtained when $Nd(Mg_{0.5}Sn_{0.5})O_3$ ceramics were sintered at 1550 °C for 4 h [8]. A dielectric constant around 18.9, a $Q \times f$ of 32,300 GHz, and a temperature coefficient of resonant frequency of -52 ppm/°C were obtained for 0.25 wt% B_2O_3-doped $Nd(Mg_{0.5}Sn_{0.5})O_3$ ceramics that were sintered at 1500 °C for 4 h [9]. Several solid solutions combining two compounds were found to have a higher value of $Q \times f$ compared with that of both end members [10–12], this phenomenon motivates this study of the effect of the substitution of Sn^{4+} (0.069 nm) by Ti^{4+} (0.0605 nm) to form $Nd(Mg_{0.5}Sn_{0.5-x}Ti_x)O_3$ ceramics [13]. In this investigation, $Nd(Mg_{0.5}Sn_{0.5-x}Ti_x)O_3$ ceramics were synthesized and some of the Sn^{4+} ions were substituted with Ti^{4+} ions to improve their $Q \times f$. Additionally, the effect of the sintering temperature on the microwave dielectric properties of $Nd(Mg_{0.5}Sn_{0.5-x}Ti_x)O_3$ ceramics was explored. $Nd(Mg_{0.5}Sn_{0.5-x}Ti_x)O_3$ ceramics were synthesized using the conventional mixed-oxide method and demonstrated to have better $Q \times f$ than that of $Nd(Mg_{0.5}Sn_{0.5})O_3$ ceramics. The microwave dielectric properties of the $Nd(Mg_{0.5}Sn_{0.5-x}Ti_x)O_3$ ceramics were found to vary with the extent of Ti^{4+} substitution and sintering temperatures. These various microwave dielectric properties were analyzed by densification, X-ray diffraction (XRD) patterns, and observation of their microstructures.

2. Experimental procedure

The starting raw chemicals were highly pure Nd_2O_3 (99.99%), MgO (98.0%), SnO_2 (99.0%), and TiO_2 (99.9%) powders. The prepared compositions corresponded to the general formula $Nd(Mg_{0.5}Sn_{0.5-x}Ti_x)O_3$. Specimens were prepared using the conventional mixed-oxide method. The raw material was weighed out in stoichiometric proportions, ball-milled in alcohol for 12 h, dried, and then calcined at

* Corresponding author. Tel.: +886 2 8209 3211; fax: +886 2 8209 9728.
E-mail addresses: EE049@mail.lhu.edu.tw, ycchenncku@yahoo.com.tw (Y.-C. Chen).

0272-8842/$36.00
doi:10.1016/j.ceramint.2011.11.069

1200 °C for 4 h. The calcined powder was re-milled for 12 h using PVA solution as a binder. The obtained fine powder was then crushed into a finer powder through a sieve with a 200 mesh. This finer powder was then axially pressed at 2000 kg/cm^2 into pellets with a diameter of 11 mm and a thickness of 6 mm. The specimens thus obtained were then heat-treated at 600 °C for 4 h to eliminate the PVA, before being sintered at temperatures of 1450–1650 °C for 4 h in air. Both the heating rate and the cooling rate were set to 10 °C/min.

Following sintering, the phases of the samples were investigated by X-ray diffraction. An X-ray Rigaku D/MAX-2200 was utilized with Cu$K\alpha$ radiation (at 30 kV and 20 mA) and a graphite monochromator in the 2θ range of 10°–80°. The polished samples were thermally etched at a temperature 100 °C below that of sintering temperature. Scanning electron microscopy (SEM; JEOL JSM-6500F, Japan) and energy dispersive X-ray spectrometer (EDS) were carried out to examine the microstructures of the specimens. The grain sizes were measured by line intercept method. The apparent densities of the specimens were measured using the liquid Archimedes method using distilled water. The A&D GF-300 Digital Scale was used to measure the apparent densities. The precision of A&D GF-300 Digital Scale is 0.001 g. The microwave dielectric properties of the specimens were measured by the postresonator method that was developed by Hakki and Coleman [14]. This method employs a specimen in the form of a cylinder of diameter D and length L. The cylindrical resonator was polished using fine emery paper to make the surfaces flat, smooth, and parallel; it was then washed with acetone in an ultra sonic bath for measurements. The cylindrical resonator was sandwiched between two finely polished brass plates. The specimens whose microwave dielectric property were measured had an aspect ratio D/L of approximately 1.6, which is in the permitted range that was determined by Kobayashi and Katoh [15]. The cylindrical resonator was sandwiched between two conducting plates. Two small antennas were positioned in the vicinity of the specimen to couple the microwave signal power into or out of the resonator. The other ends of the antennas were connected to an Agilent E5071C network analyzer (Agilent Technologies Inc., Santa Clara, CA). The resonance characteristics depended on the size and the microwave dielectric properties of the specimen. The microwave energy was coupled using electric-field probes. The TE_{011} resonant mode was optimal for determining the dielectric constant and the loss factor of the specimen. The Agilent E5071C network analyzer was adopted to identify the TE_{011} resonant frequency of the dielectric resonator, and the dielectric constant and quality factor were calculated. The conductor loss of the end plates must be subtracted to obtain the quality factor. For this purpose, two specimens with different heights were prepared, where the height of the specimen for the TE_{012} mode measurement was twice as large as that of the specimen for the TE_{011} mode. The approach for measuring τ_f was the same as that for measuring the dielectric constant. The test cavity was placed in a chamber and the temperature was increased from 25 to 75 °C. The τ_f value (ppm/°C) was determined from the change in resonant frequency:

$$\tau_f = \frac{f_2 - f_1}{f_1(T_2 - T_1)}, \tag{1}$$

where f_1 and f_2 denote the resonant frequencies at T_1 and T_2, respectively.

3. Results and discussion

Fig. 1 presents the X-ray diffraction patterns of $Nd(Mg_{0.5}Sn_{0.4}Ti_{0.1})O_3$ ceramics that were sintered at 1450–1650 °C for 4 h. Small amount of $Nd_2Sn_2O_7$ as the second phase is accompanied. $Nd_2Sn_2O_7$ with cubic crystal structure (ICDD-PDF #88–0448) was identified and difficult to completely eliminate from the sample prepared by mixed oxide route. As shown in Fig. 1, the (2 2 2) and (4 0 0) peaks of the $Nd_2Sn_2O_7$ ceramics were at 29.253° and 33.905°, respectively. The formation of the Sn-rich second phase $Nd_2Sn_2O_7$ was attributed to the loss of MgO upon ignition. The formation of $Nd_2Sn_2O_7$ might deteriorate the dielectric constant and quality factor of the specimen. A later investigation will involve preparation of the powder by precipitation from solution. Such a method may yield a single-phase product. A single-phase product potentially has much higher values of the parameters of interest. A series of extra peaks were observed to correspond to superlattice reflections. All of the superlattice reflections were indexed using half integer Miller indices. According to Glazer, the

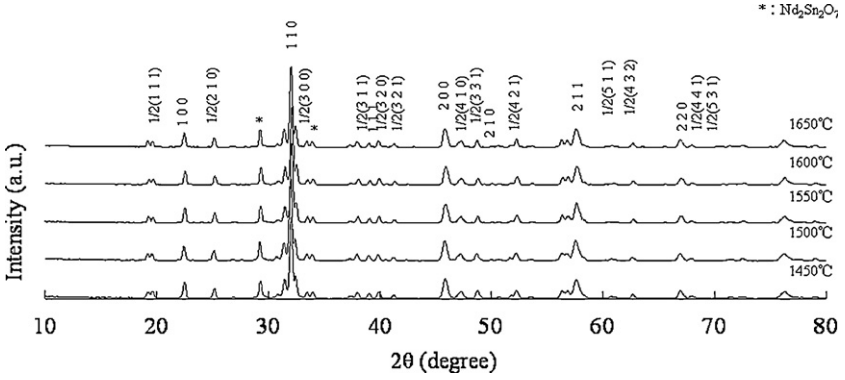

Fig. 1. X-ray diffraction patterns of $Nd(Mg_{0.5}Sn_{0.4}Ti_{0.1})O_3$ ceramics sintered at 1450–1650 °C for 4 h.

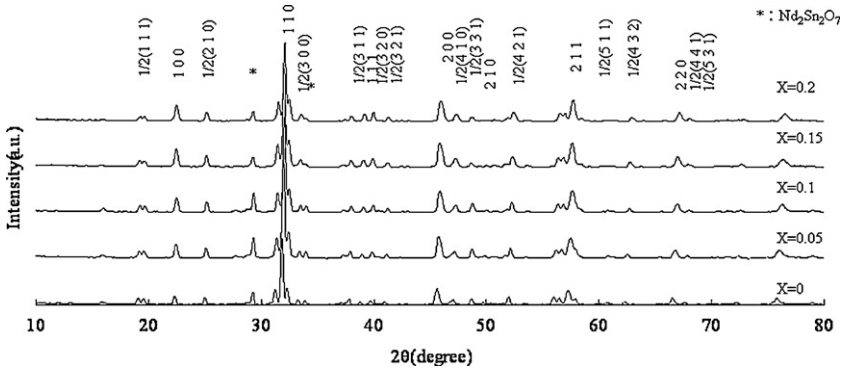

Fig. 2. X-ray diffraction patterns of $Nd(Mg_{0.5}Sn_{0.5-x}Ti_x)O_3$ specimens sintered at 1550 °C for 4 h with x varied from 0 to 0.2.

superlattice reflections, with specific combinations of odd (o) and even (e) Miller indices, reveal particular deviations of the structure from the undistorted cubic structure, such as octahedral in-phase tilting (o o e, o e o, e o o), anti-phase tilting (o o o, $h + k + l > 3$), and anti-parallel displacement of A-cations (e e o, e o e, o e e) [16]. The (1/2(2 1 0), 1/2(3 0 0), 1/2(3 2 0), 1/2(4 1 0), 1/2(4 2 1), 1/2(4 3 2), and 1/2(4 4 1)) extra peaks demonstrate A-site cation displacement, the (1/2(3 1 1), 1/2(3 3 1), and 1/2(5 1 1)) peaks indict anti-phase tilting, and the 1/2(3 2 1) peaks indict in-phase tilting. The 1/2(1 1 1) is evidence of 1:1 B-site cation ordering. The X-ray diffraction patterns of the $Nd(Mg_{0.5}Sn_{0.4}Ti_{0.1})O_3$ ceramics do not significantly vary with sintering temperature. Fig. 2 shows the X-ray diffraction patterns of $Nd(Mg_{0.5}Sn_{0.5-x}Ti_x)O_3$ ceramics with x varied from 0 to 0.2, following sintering at 1550 °C for 4 h. The diffraction peaks of $Nd(Mg_{0.5}Sn_{0.5-x}Ti_x)O_3$ ceramics shifted to higher angles as x increased, perhaps because the ionic radius of Ti^{4+} ions (0.0605 nm) is smaller than that of Sn^{4+} ions (0.069 nm). As shown in Table 1, the tolerance factors of $Nd(Mg_{0.5}Sn_{0.5-x}Ti_x)O_3$ ceramics increased from 0.8970 to 0.9043 as x increased from 0 to 0.2. The tolerance factor was calculated using the ionic radius data of Shannon [13]. The tolerance factors of $Nd(Mg_{0.5}Sn_{0.5-x}Ti_x)O_3$ series are in the anti-phase and in-phase titled region [17], which is in agreement with those of X-ray diffraction patterns. The perovskite cell deformed and symmetry lowered from cubic when tolerance factor deviated from one. Deviation from cubic symmetry resulted in extra polarizations, which reflected in the dielectric constant, and, therefore, a higher dielectric constant [18]. The amount of main phase was evaluated from most intensive lines of main and second phases,

$$Nd(Mg_{0.5}Sn_{0.5-x}Ti_x)O_3\ (\text{vol}\%) = \frac{I_{A(1\,1\,0)}}{I_{A(1\,1\,0)} + I_{B(2\,2\,2)}} \times 100, \quad (2)$$

where I_A and I_B are the most intensive line of $Nd(Mg_{0.5}Sn_{0.5-x}Ti_x)O_3$ (1 1 0) and $Nd_2Sn_2O_7$ (2 2 2), respectively. As shown in Table 2, the amount of main phase stabled as x increased from 0 to 0.05, then increased from 82.09% to 90.55% as x increased from 0.05 to 0.15, and stabled as x varied from 0.15 to 0.2. The formation of second phase of $Nd_2Sn_2O_7$ affected the apparent density and microwave dielectric properties of $Nd(Mg_{0.5}Sn_{0.5-x}Ti_x)O_3$ ceramics.

Fig. 3 shows the thermally etched surfaces of $Nd(Mg_{0.5}Sn_{0.5-x}Ti_x)O_3$ ceramics following sintering for 4 h at various temperatures. The microstructures of $Nd(Mg_{0.5}Sn_{0.5-x}Ti_x)O_3$ ceramics when Sn^{4+} ions were replaced

Table 1
Tolerance factor, main phase (%), second phase (%), theoretical density, relative density, and internal strain of $Nd(Mg_{0.5}Sn_{0.5-x}Ti_x)O_3$ ceramics.

x	Tolerance factor	Main phase (%)	Second phase (%)	Theoretical density (g/cm^3)	Relative density	Internal strain
0	0.8970	83.57	16.43	7.00	99.6	0.011
0.05	0.8989	82.09	17.91	7.00	98.8	0.012
0.1	0.9007	82.20	17.80	6.94	98.4	0.009
0.15	0.9025	90.55	9.45	6.90	97.9	0.011
0.2	0.9043	88.33	11.67	6.85	97.0	0.012

Table 2
EDS data of grains of $Nd(Mg_{0.5}Sn_{0.4}Ti_{0.1})O_3$ ceramics sintered at 1550 °C for 4 h.

Atomic element	Nd (%)	Mg (%)	Sn (%)	Ti (%)	O (%)
A	14.43	6.99	6.35	2.40	69.82
B	12.02	6.86	5.28	1.01	74.83
C	10.07	0	0	8.87	81.06

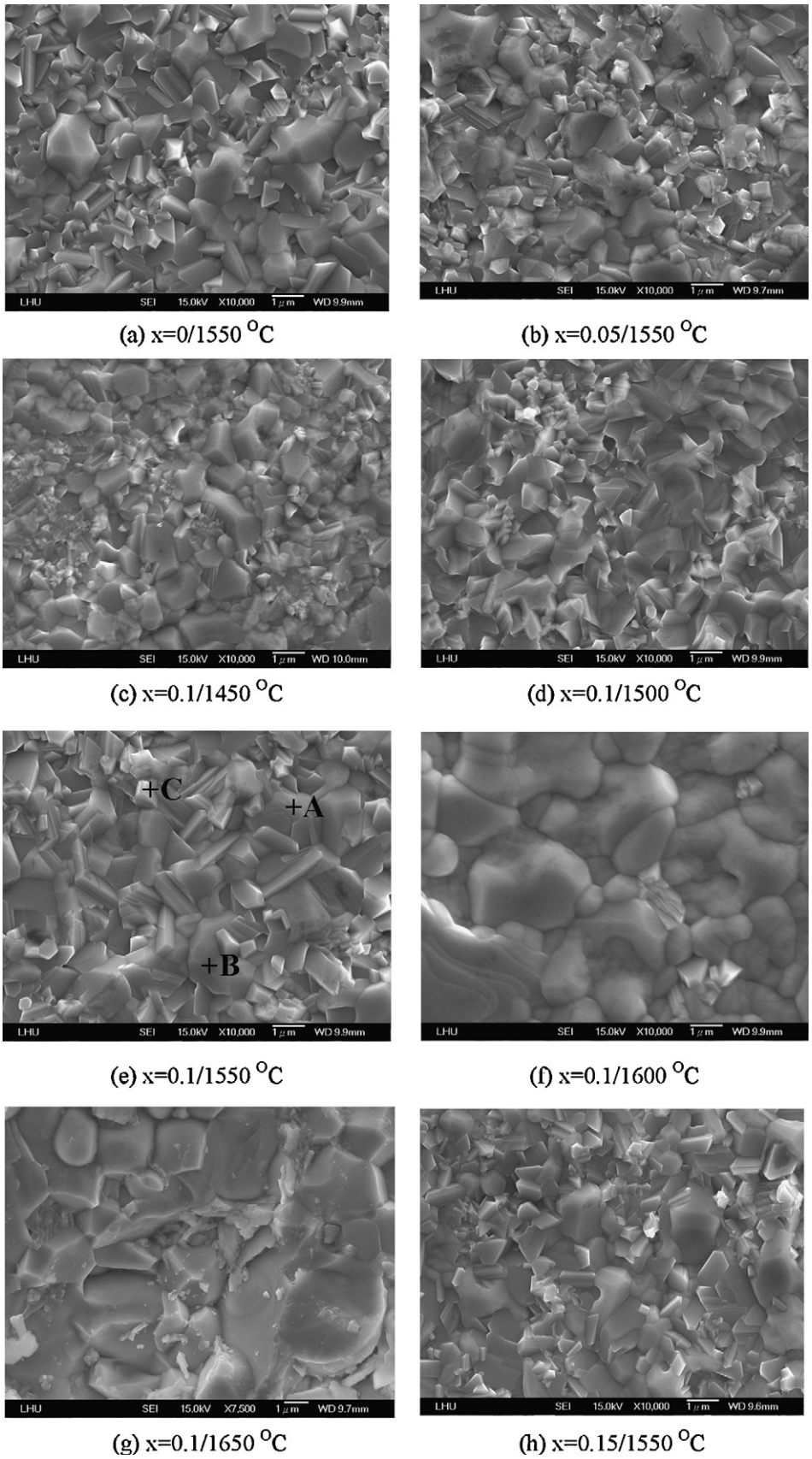

Fig. 3. Microstructures of $Nd(Mg_{0.5}Sn_{0.5-x}Ti_x)O_3$ ceramics sintered under different temperatures for 4 h: (a) $x = 0$/1550 °C, (b) $x = 0.05$/1550 °C, (c) $x = 0.1$/1450 °C, (d) $x = 0.1$/1500 °C, (e) $x = 0.1$/1550 °C, (f) $x = 0.1$/1600 °C, (g) $x = 0.1$/1650 °C, (h) $x = 0.15$/1550 °C, and (i) $x = 0.2$/1500 °C.

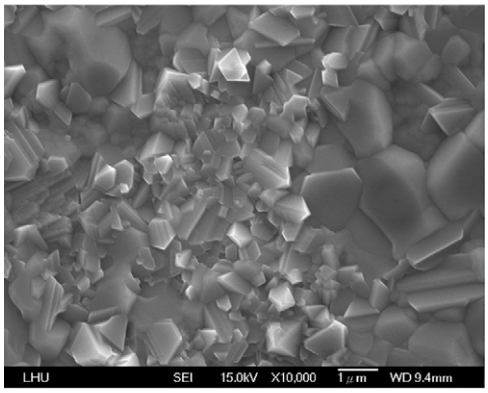

(i) x=0.2/1550 °C

Fig. 3. (*Continued*).

with different degrees of Ti^{4+} substitution indicated that the average grain size did not vary significantly with the extent of Ti^{4+} substitution. Comparing the microstructures of $Nd(Mg_{0.5}Sn_{0.4}Ti_{0.1})O_3$ ceramics that were sintered under different temperatures indicated that the average grain size of the $Nd(Mg_{0.5}Sn_{0.4}Ti_{0.1})O_3$ ceramics increased from 0.88 to 2.33 μm as the temperature of sintering for 4 h increased from 1450 to 1650 °C. To identify the composition of the second phase, an energy-disperse spectroscopy (EDS) analysis was carried out on the grains of $Nd(Mg_{0.5}Sn_{0.4}Ti_{0.1})O_3$ ceramics that were sintered at 1550 °C for 4 h, as shown in Fig. 3(e). According to the quantitative analysis, which is shown in Table 2, A and B grains are evidently $Nd(Mg_{0.5}Sn_{0.4}Ti_{0.1})O_3$ and the C grain is $Nd_2Sn_2O_7$.

Fig. 4 shows the selected area electron diffraction pattern (SEAD) of $Nd(Mg_{0.5}Sn_{0.4}Ti_{0.1})O_3$ ceramic that were sintered at 1550 °C. The SAED pattern was composed of concentric rings of bright spots. The SAED pattern shows the character of polycrystalline. Electron beam diffracts from the crystallographic planes of the unit cells composing the specimen. The interpreted patterns of number 1, 2, 3, 4, 5, and 6 corresponded to the (1 0 0), (1 1 0), (2 0 0), (2 1 1), 1/2(3 1 1), and 1/2(3 2 0) planes, respectively.

Fig. 5 shows the apparent densities of the $Nd(Mg_{0.5}Sn_{0.5-x}Ti_x)O_3$ ceramics with different degrees of Ti^{4+} substitution, following sintering at 1450–1650 °C for 4 h. The apparent density of the $Nd(Mg_{0.5}Sn_{0.4}Ti_{0.1})O_3$ ceramics that were sintered at 1450–1650 °C for 4 h was greatest when sintering was carried out at 1550 °C, beyond which temperature, the apparent density decreased. The decrease in the number of pores may have been responsible for the increase in apparent density, as shown in Fig. 3. The maximum apparent density of the $Nd(Mg_{0.5}Sn_{0.5-x}Ti_x)O_3$ ceramics sintered at 1550 °C for 4 h decreased from 7.0 to 6.6 g/cm^3 as x increased from 0 to 0.2. Since the Ti atom has a smaller mass than that of the Sn atom, the apparent density of $Nd(Mg_{0.5}Sn_{0.5-x}Ti_x)O_3$ ceramics is expected to be decreased as x increased. The optimum sintering temperature of the $Nd(Mg_{0.5}Sn_{0.5-x}Ti_x)O_3$ ceramics decreased from 1550 to 1500 °C as x increased from 0.1 to 0.15. The theoretical density of the composites can be calculated by following equation:

$$D_{\text{composite}} = V_1 D_1 + V_2 D_2, \quad (3)$$

where $D_{\text{composite}}$ is the calculated theoretical density of the composite, V_1 and V_2 are the volume fraction of

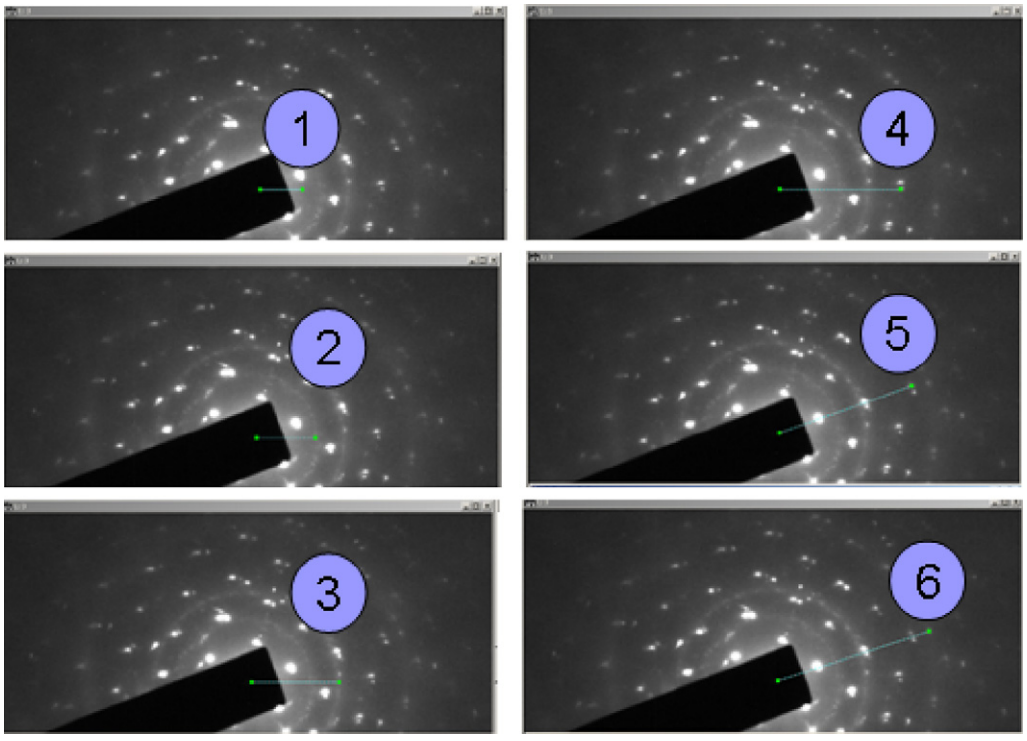

Fig. 4. Selected area electron diffraction pattern (SEAD) of $Nd(Mg_{0.5}Sn_{0.4}Ti_{0.1})O_3$ ceramic that were sintered at 1550 °C.

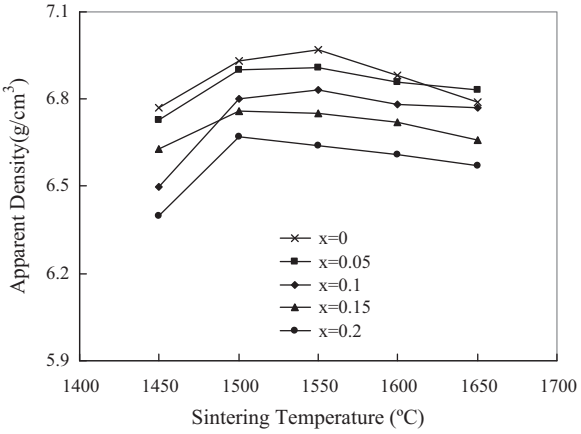

Fig. 5. Apparent densities of $Nd(Mg_{0.5}Sn_{0.5-x}Ti_x)O_3$ ceramics with various degrees of Ti^{4+} substitution, following sintering at various temperatures for 4 h.

$Nd(Mg_{0.5}Sn_{0.5-x}Ti_x)O_3$ and $Nd_2Sn_2O_7$, respectively, and D_1 and D_2 are the theoretical density of $Nd(Mg_{0.5}Sn_{0.5-x}Ti_x)O_3$ and $Nd_2Sn_2O_7$, respectively. Table 1 shows the theoretical density and relative density of $Nd(Mg_{0.5}Sn_{0.5-x}Ti_x)O_3$ ceramics with different degrees of Ti^{4+} substitution, following sintering at 1550 °C for 4 h. The relative densities of $Nd(Mg_{0.5}Sn_{0.5-x}Ti_x)O_3$ ceramics that were sintered at 1550 °C for 4 h decreased from 99.63% to 96.97% as x increased from 0 to 0.2.

Fig. 6 shows the dielectric constants of $Nd(Mg_{0.5}Sn_{0.5-x}Ti_x)O_3$ ceramics with different degrees of Ti^{4+} substitution, following sintering at 1450–1650 °C for 4 h. $Nd(Mg_{0.5}Sn_{0.3}Ti_{0.2})O_3$ ceramics that were sintered at 1500 °C for 4 h had a maximum dielectric constant of 22.8. A high dielectric constant of $Nd(Mg_{0.5}Sn_{0.3}Ti_{0.2})O_3$ ceramics that were sintered at 1500 °C for 4 h did not depend on a high sintering temperature. The decrease in dielectric constant was associated with low apparent densities of the ceramics. A higher density is associated with lower porosity, and, therefore, a higher dielectric constant. The dielectric constant of the composites can be calculated by the mixture rule:

$$\log \varepsilon_r = V_1 \log \varepsilon_{r1} + V_2 \log \varepsilon_{r2}, \quad (4)$$

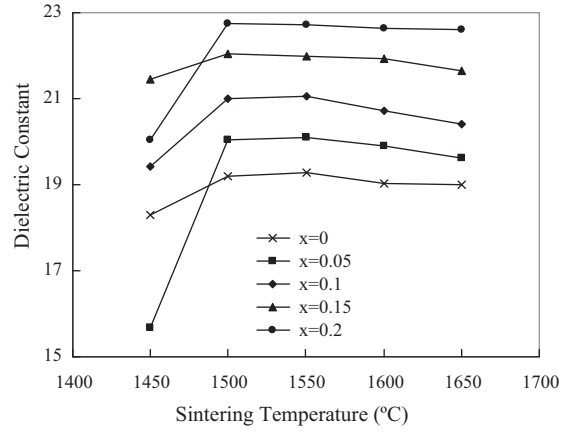

Fig. 6. Dielectric constants of $Nd(Mg_{0.5}Sn_{0.5-x}Ti_x)O_3$ ceramics with various degrees of Ti^{4+} substitution, following sintering at various temperatures for 4 h.

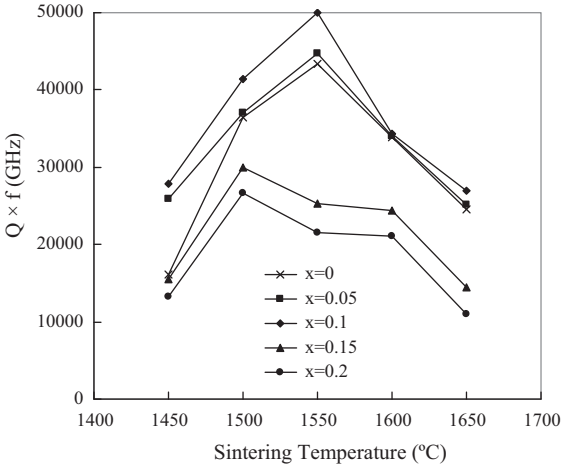

Fig. 7. Q × f of $Nd(Mg_{0.5}Sn_{0.5-x}Ti_x)O_3$ ceramics with various degrees of Ti^{4+} substitution, following sintering at various temperatures for 4 h.

where ε_r is the dielectric constant of the composite, V_1 and V_2 are the volume fraction of $Nd(Mg_{0.5}Sn_{0.5-x}Ti_x)O_3$ and $Nd_2Sn_2O_7$, respectively, and ε_{r1} and ε_{r2} are the dielectric constant of $Nd(Mg_{0.5}Sn_{0.5-x}Ti_x)O_3$ and $Nd_2Sn_2O_7$, respectively. Since the dielectric constant of $Nd_2Sn_2O_7$ ceramics was 17.0 as shown in Table 3, the appearance of $Nd_2Sn_2O_7$ deteriorated the dielectric constants of specimens. The dielectric constant of $Nd(Mg_{0.5}Sn_{0.5-x}Ti_x)O_3$ ceramics increased from 19.3 to 22.7 as x increased from 0 to 0.2 when the $Nd(Mg_{0.5}Sn_{0.5-x}Ti_x)O_3$ ceramics were sintered at 1550 °C for 4 h. Although the relative density decreased as x increased as shown in Table 1, the dielectric constant of $Nd(Mg_{0.5}Sn_{0.5-x}Ti_x)O_3$ ceramics increased as x increased from 0 to 0.2. This fact may be explained by the molar volume and ionic polarization, as suggested by Tohto et al. [19] the dielectric constant can be calculated using the Clausius–Mossotti equation:

$$\varepsilon_r = \frac{3V_m + 8\pi\alpha_D}{3V_m - 4\pi\alpha_D} \quad (5)$$

where V_m represents the molar volume and α_D is the sum of the ionic polarizabilities of individual ions. The dielectric constant calculated by Eq. (5) was intrinsic factor to dielectric property. Dielectric constants therefore depend on the molar volume and ionic polarization. As indicated by Eq. (5), a smaller molar volume or a larger ionic polarization is associated with a larger dielectric constant. The influence of ionic polarization on dielectric constant is much larger than that of molar volume. The ionic polarization of Ti^{4+} ion and Sn^{4+} ions are 2.93 and 2.83 $Å^3$, respectively [20,21]. The sum of ionic polarizations of individual ions of $Nd(Mg_{0.5}Sn_{0.5-x}Ti_x)O_3$ ceramics increased as x in-

Table 3
Microwave Dielectric Properties of $Nd_2Sn_2O_7$ ceramics sintered at 1550 °C for 9 h.

Apparent density (g/cm^3)	ε_r	Q × f (GHz)	τ_f (ppm/°C)
7.11	17.0	33,100	−55

creased, so the dielectric constant of $Nd(Mg_{0.5}Sn_{0.5-x}Ti_x)O_3$ ceramics is expected to be increased as x increased.

Fig. 7 shows the $Q \times f$ of the $Nd(Mg_{0.5}Sn_{0.5-x}Ti_x)O_3$ ceramics with different degrees of Ti^{4+} substitution, following sintering at 1450–1650 °C for 4 h. The relationship between the $Q \times f$ and the sintering temperature of $Nd(Mg_{0.5}Sn_{0.4}Ti_{0.1})O_3$ ceramics was consistent with that between the apparent density and the sintering temperature, because the microwave dielectric loss is affected by many factors, which is composed of intrinsic and extrinsic losses. Intrinsic loss is associated with the vibration modes of the lattice. Extrinsic loss is associated with the density, porosity, second phases, impurities, oxygen vacancies, grain size, and lattice defects [22,23]. A $Q \times f$ of 33,100 GHz was obtained for $Nd_2Sn_2O_7$ ceramics as shown in Table 3. The appearance of $Nd_2Sn_2O_7$ worsened the $Q \times f$ of $Nd(Mg_{0.5}Sn_{0.5-x}Ti_x)O_3$ ceramics. Since the $Q \times f$ of $Nd(Mg_{0.5}Sn_{0.4}Ti_{0.1})O_3$ ceramics was consistent with the variation of the apparent density, the $Q \times f$ of $Nd(Mg_{0.5}Sn_{0.4}Ti_{0.1})O_3$ ceramics is suggested to be dominated by the apparent density. $Nd(Mg_{0.5}Sn_{0.4}Ti_{0.1})O_3$ ceramics that were sintered at 1550 °C for 4 h had a maximum $Q \times f$ of 50,000 GHz in the series of $Nd(Mg_{0.5}Sn_{0.5-x}Ti_x)O_3$ ceramics. The results suggest that the $Q \times f$ increased by partially substituting Sn^{4+} ions with Ti^{4+} ions. This fact may be explained by the relative density and internal strain. Densification plays an important role in controlling the $Q \times f$ as described above. The relative density of $Nd(Mg_{0.5}Sn_{0.5-x}Ti_x)O_3$ ceramics decreased as x increased as shown in Table 1. However, the $Q \times f$ of specimens increased as x increased from 0 to 0.1. The increase in $Q \times f$ values with x when $x \leq 0.1$, then decrease with x when $x > 0.1$ was associated with the internal strain. The internal strain η can be calculated by following equation, as suggested by Stokes et al. [24].

$$\beta = 2\eta \tan\theta, \tag{6}$$

where β is the full width at half maximum (FWHM) of X-ray diffraction peaks, θ is the diffraction angles. Curve fitting was used to fit the internal strain η of $Nd(Mg_{0.5}Sn_{0.5-x}Ti_x)O_3$ ceramics with different degrees of Ti^{4+} substitution sintered at 1550 °C for 4 h with Eq. (6). The curve fittings employed were based on the least-squares method. In this method, the square of the deviation of the experimental value from the theoretical expectation was calculated while varying the fitted internal strain. The fitting process was ended at a specific value of the fitted internal strain where the deviation was minimized. Table 1 shows the internal strain of $Nd(Mg_{0.5}Sn_{0.5-x}Ti_x)O_3$ ceramics with different degrees of Ti^{4+} substitution. $Nd(Mg_{0.5}Sn_{0.4}Ti_{0.1})O_3$ ceramics had a minimum internal strain of 0.009 in the series of $Nd(Mg_{0.5}Sn_{0.5-x}Ti_x)O_3$ ceramics. The $Q \times f$ of $Nd(Mg_{0.5}Sn_{0.5-x}Ti_x)O_3$ ceramics is inferred to be controlled by the internal strain.

Fig. 8 shows the temperature coefficient of resonant frequency (τ_f) of $Nd(Mg_{0.5}Sn_{0.5-x}Ti_x)O_3$ ceramics with different degrees of Ti^{4+} substitution, following sintering at 1450–1650 °C for 4 h. Generally, τ_f is related to the composition and the degrees of second phase that are presented in the ceramics. Since the composition of $Nd(Mg_{0.5}Sn_{0.5-x}Ti_x)O_3$ ceramics with a fixed degrees of Ti^{4+} substitution did not vary with sintering

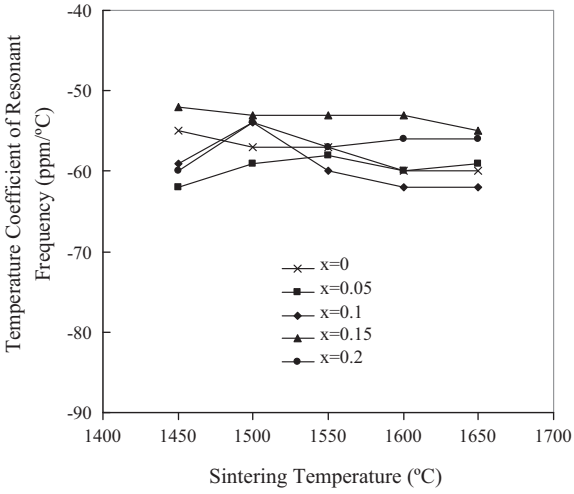

Fig. 8. τ_f of $Nd(Mg_{0.5}Sn_{0.5-x}Ti_x)O_3$ ceramics with various degrees of Ti^{4+} substitution, following sintering at various temperatures for 4 h.

temperature, no significant variation in τ_f of $Nd(Mg_{0.5}Sn_{0.5-x}Ti_x)O_3$ ceramics with sintering temperature over the entire range of sintering temperatures considered herein was observed. As shown in Table 3, a τ_f of −55 ppm/°C was obtained for $Nd_2Sn_2O_7$ ceramics. The τ_f of $Nd_2Sn_2O_7$ ceramics is compatible with that of $Nd(Mg_{0.5}Sn_{0.5-x}Ti_x)O_3$ ceramics, implying the presence of the second phase will not bring much deviation to the τ_f of the specimen. A τ_f of −60 ppm/°C was measured for $Nd(Mg_{0.5}Sn_{0.4}Ti_{0.1})O_3$ ceramics that was sintered at 1550 °C for 4 h.

4. Conclusions

The effects of the degree of Ti^{4+} substitution and sintering temperature on the microwave dielectric properties of $Nd(Mg_{0.5}Sn_{0.5-x}Ti_x)O_3$ ceramics were explored. $Nd(Mg_{0.5}Sn_{0.4}Ti_{0.1})O_3$ ceramics that were sintered at 1550 °C for 4 h had a dielectric constant of 21.1, a $Q \times f$ of 50,000 GHz, and a temperature coefficient of resonant frequency (τ_f) of −60 ppm/°C. The appearance of $Nd_2Sn_2O_7$ declined the dielectric constant and $Q \times f$ of $Nd(Mg_{0.5}Sn_{0.5-x}Ti_x)O_3$ ceramics. The dielectric constant of $Nd(Mg_{0.5}Sn_{0.5-x}Ti_x)O_3$ ceramics was affected by the density, molar volume, and ionic polarization. The $Q \times f$ of $Nd(Mg_{0.5}Sn_{0.5-x}Ti_x)O_3$ ceramics depended on the density and internal strain.

Acknowledgment

The authors would like to thank the National Science Council in Taiwan, for financially supporting this research under Contract No. NSC 100-2622-E-262-001-CC3.

References

[1] C.L. Huang, J.J. Wang, B.J. Li, W.C. Lee, Effect of B_2O_3 additives on sintering and microwave dielectric behaviors of $0.66Ca(Mg_{1/3}Nb_{2/3})O_3$–$0.34CaTiO_3$ ceramics, J. Alloys Compd. 461 (2008) 440–446.

[2] Y.C. Chen, W.Y. Hsu, Dielectric properties of CuO-doped $La_{2.98/3}Ba_{0.01}(Mg_{0.5}Sn_{0.5})O_3$ ceramics at microwave frequency, Ceram. Int. 37 (2010) 55–58.
[3] C.L. Huang, R.J. Lin, J.F. Tseng, Dielectric properties of copper oxide doped $0.95Ba(Zn_{1/3}Ta_{2/3})O_3$–$0.05BaZrO_3$ ceramics at microwave frequency, Mater. Chem. Phys. 97 (2006) 256–260.
[4] N. Ichinose, T. Shimada, Effect of grain size and secondary phase on microwave dielectric properties of $Ba(Mg_{1/3}Ta_{2/3})O_3$ and $Ba([Mg,Zn]_{1/3}Ta_{2/3})O_3$ systems, J. Eur. Ceram. Soc. 26 (2006) 1755–1759.
[5] C.H. Hsu, C.F. Shih, C.C. Yu, H.H. Tung, M.H. Chung, Low temperature sintering and microwave dielectric properties of $0.6Ba(Co_{1/3}Nb_{2/3})O_3$–$0.4Ba(Ni_{1/3}Nb_{2/3})O_3$ ceramics using copper additions, J. Alloys Compd. 461 (2008) 355–359.
[6] W.C. Tzou, Y.S. Yang, C.F. Yang, H.H. Chung, C.J. Huang, C.C. Diao, Microstructure and microwave dielectric characteristics of $(1-x)Ba(Zn_{1/3}Ta_{2/3})O_3$–$xBaTi_4O_9$ ceramics, Mater. Res. Bull. 42 (2007) 1897–1904.
[7] M.T. Sebastian, K.P. Surendran, Tailoring the microwave dielectric properties of $Ba(Mg_{1/3}Ta_{2/3})O_3$ ceramics, J. Eur. Ceram. Soc. 26 (2006) 1791–1799.
[8] Y.C. Chen, R.J. Tsai, Effect of sintering temperature and time on microwave dielectric properties of $Nd(Mg_{0.5}Sn_{0.5})O_3$ ceramics, Mater. Chem. Phys. 129 (2011) 116–120.
[9] Y.C. Chen, R.J. Tsai, Y.N. Wang, Dielectric properties of B_2O_3-doped $Nd(Mg_{0.5}Sn_{0.5})O_3$ ceramics at microwave frequencies, Ferroelectrics 396 (2011) 104–112.
[10] C.L. Huang, C.Y. Tai, C.Y. Huang, Y.H. Chien, Low-loss microwave dielectrics in the spinel-strutured $(Mg_{1-x}Ni_x)Al_2O_4$ solid solutions, J. Am. Ceram. Soc. 93 (2010) 1999–2003.
[11] T. Oishi, A. Kan, H. Ohsato, H. Ogawa, Crystal structure-microwave dielectric property relations in $Sm(Nb_{1-x}Ta_x)(Ti_{1-y}Zr_y)O_6$ ceramics, J. Eur. Ceram. Soc. 26 (2006) 2075–2079.
[12] S.F. Wang, Y.F. Hsu, Y.R. Wang, L.T. Cheng, Y.C. Hsu, J.P. Chu, C.Y. Huang, Densification, microstructural evolution and dielectric properties of $Ba_{6-3x}(Sm_{1-y}Nd_y)_{8+2x}Ti_{18}O_{54}$ microwave ceramics, J. Eur. Ceram. Soc. 26 (2006) 1629–1635.
[13] R.D. Shannon, Revised effective ionic radii in halides and chalcogenides, Acta Crystallogr. A32 (1976) 751–767.
[14] B.W. Hakki, P.D. Coleman, A dielectric resonator method of measuring inductive capacities in the millimeter range, IEEE Trans. Microw. Theory Technol. 8 (1960) 402–410.
[15] Y. Kobayashi, M. Katoh, Microwave measurement of dielectric properties of low-loss materials by the dielectric rod resonator method, IEEE Trans. Microw. Theory Technol. 33 (1985) 586–592.
[16] A.M. Glazer, Simple ways of determining perovskite structures, Acta Crystallogr. A31 (1975) 756–762.
[17] I.M. Reaney, E.L. Collea, N. Setter, Dielectric and structural characteristics of Ba- and Sr-based complex perovskites as a function of tolerance factor, Jpn. J. Appl. Phys. 33 (1994) 3984–3990.
[18] E.S. Kim, Y.H. Kim, J.H. Chae, D.W. Kim, K.H. Yoon, Dielectric properties of $[(Pb_{0.2}Ca_{0.8})_{1-x}Sr_x](Ca_{1/3}Nb_{2/3})O_3$ ceramics at microwave frequencies, Mater. Phys. Chem. 79 (2003) 230–232.
[19] Y. Tohdo, K. Kakimoto, H. Ohsato, H. Yamada, T. Okawa, Microwave dielectric properties and crystal structure of homologous compounds $ALa_4Ti_4O_{15}$ (A = Ba, Sr and Ca) for base station applications, J. Eur. Ceram. Soc. 26 (2006) 2039–2043.
[20] R.D. Shannon, Dielectric polarizabilities of ions in oxides and fluorides, J. Appl. Phys. 73 (1993) 348–366.
[21] C. Veneis, P.K. Davies, T. Negas, S. Bell, Microwave dielectric properties of hexagonal perovskites, Mater. Res. Bull. 31 (1996) 431–437.
[22] B.D. Silverman, Microwave absorption in cubic strontium titanate, Phys. Rev. 125 (1962) 1921–1930.
[23] W.S. Kim, T.H. Hong, E.S. Kim, K.H. Yoon, Microwave dielectric properties and far infrared reflectivity spectra of the $(Zr_{0.8}Sn_{0.2})TiO_4$ ceramics with additives, Jpn. J. Appl. Phys. 37 (1998) 3567–3571.
[24] H. Ohsato, M. Imaeda, The quality factor of the microware dielectric materials based on the crystal structure – as an example: the $Ba_{6-3x}R_{8+2x}$-$Ti_{18}O_{54}$ (R = rare earth) solid solutions, Mater. Chem. Phys. 79 (2003) 208–212.